

# Variability in Footpoint Mapping of BBFs Using Tsyganenko Models: Impact on Swarm Conjunctions

V. Lanabere<sup>1,\*</sup>, A. P. Dimmock<sup>1</sup>, L. Richard<sup>1</sup>, S. Buchert<sup>1</sup>, Y. V. Khotyaintsev<sup>1</sup>,  
and O. Marghita<sup>2</sup>

<sup>1</sup> Swedish Institute of Space Physics, Institutet för rymdfysik Box 537, 751 21 Uppsala, Sweden

<sup>2</sup> Institute of Space Science, Bucharest, Măgurele 077125, Rumania

## ABSTRACT

Magnetospheric-ionospheric coupling studies often rely on multi-spacecraft conjunctions, which require accurate magnetic field mapping tools. For example, linking measurements from the magnetotail with those in the ionosphere involves determining when the orbital magnetic footpoint of THEMIS or MMS intersects with the footpoint of Swarm. One of the most commonly used tools for tracing magnetic field lines are the Tsyganenko models. In this study, we aim to analyze how the footpoint locations are impacted by the inputs parameters of these models, including solar wind conditions, geomagnetic activity, and the location in the magnetotail. A dataset of 2394 bursty bulk flows (BBFs) detected by MMS was mapped to Earth's ionosphere with four different Tsyganenko models. The MLT position showed a variability of approximately  $\pm 1$  MLT across the models. Footpoint locations were linked to the dawn-dusk position of the BBFs, with differences between models associated with variations in the interplanetary magnetic field clock angle. The MLAT values exhibited greater variability of approximately  $\pm 2^\circ$  around the mean value, with a systematic shift toward higher latitudes observed in two of the four models. This position is also influenced by the the input parameter of the model representing the dynamics of Earth's magnetosphere, with larger values corresponding to lower latitudes. The uncertainty on the footpoint location impacts the number of conjunctions. Generally, Swarm B exhibited more conjunctions than Swarm A or C in the northern hemisphere, and less than half of these conjunctions had Tsyganenko footpoint distances below the typical BBF footprint size in the ionosphere.

**Key words.** Bursty bulk flows footpoint – Tsyganenko mapping – Field-aligned currents

## 1. Introduction

Substorms play a crucial role in the dynamics of the Earth's magnetotail, significantly influencing the transport of mass, energy, and magnetic flux. One of the key processes during substorms is the

\* Corresponding author: [vanina.lanabere@irfu.se](mailto:vanina.lanabere@irfu.se)

generation of transient high-speed plasma flows, known as bursty bulk flows (BBFs, [Angelopoulos et al., 1994](#)). These BBFs eventually couple to the high-latitude ionosphere by forming field-aligned currents (FACs) systems closed by an electrojet current in the ionosphere (e.g. [Nakamura et al., 2001](#); [Liu et al., 2015](#)). This coupling has notable ionospheric and ground magnetic manifestations, such as auroral streamers and magnetic field disturbances ( $dB/dt$ ) spikes (e.g. [Juusola et al., 2009](#); [Schillings et al., 2023](#)), which can lead to geomagnetic induced currents that have damaging effects on technological systems like power grids (e.g. [Pulkkinen et al., 2005](#); [Rodger et al., 2017](#)).

To study the ionospheric and ground manifestation of magnetotail drivers, it is essential to utilize multi-point observations (e.g. [Keiling et al., 2009](#); [Juusola et al., 2009](#); [Wei et al., 2021](#); [Aryan et al., 2022](#)). For example, linking measurements from the magnetotail to the ionosphere requires determining the times at which the orbital magnetic footprints of different spacecraft intersect. In this context, accurately mapping spacecraft positions throughout the magnetosphere to specific locations in the ionosphere is crucial. The most commonly used external magnetic field model for connecting magnetospheric substorm and storm dynamic processes to their ionospheric signatures are the Tsyganenko models ([Tsyganenko, 1987](#), hereafter T87), ([Tsyganenko, 1989](#), hereafter T89), ([Tsyganenko, 1996](#), hereafter T96), ([Tsyganenko, 2002a,b](#), hereafter T01), and ([Tsyganenko and Sitnov, 2005](#), hereafter T04). However, studies have shown limitations in these models; for example, [Opgenoorth et al. \(1994\)](#) found in their study that the presence of a localized FAC was shifted a few degrees north compared to the location obtained with the T89 model. Similarly, [Wei et al. \(2021\)](#) noted differences in the ground track mapping when using three different Tsyganenko models (T87, T89, and T96) while investigating the characteristics and responses of the magnetosphere-ionosphere-ground system during a case study.

In several studies, the spacecraft footpoint is conducted using only one mapping model (e.g. [Keiling et al., 2009](#); [Juusola et al., 2009](#); [Panov et al., 2019](#)). It is acceptable when ionospheric and ground signatures are distinct enough to confidently attribute them to a specific magnetotail driver. However, in many cases, the true footpoint remains uncertain, or it may be impractical to validate every conjunction individually, particularly in statistical studies that involve extensive mapping. This uncertainty raises the importance of accurately defining what constitutes a conjunction in such contexts.

This study utilizes a large database of BBF events observed by the Magnetospheric Multiscale (MMS) spacecraft ([Burch et al., 2016](#)) to statistically compare the mapped footpoint locations among four different Tsyganenko models. We refer to the footpoint as a unique point representing the BBF and do not consider the spatial size of the BBF mapped into the ionosphere (footprint). In this work, we do not address the error in footpoint location, as establishing a ground truth for the correct footpoint for each event is necessary and beyond the scope of this analysis. Instead we analyze how the footpoint locations are impacted by the inputs parameters of these models, including solar wind conditions, geomagnetic activity, the location of the BBF in the magnetotail, and the tilt angle. We report how the number of conjunction between BBFs and Swarm spacecraft changes when the conjunction definition is adjusted. Specifically, we examine how increasing the time interval between the detection of BBF and the Swarm satellites' path through the BBF footpoint, as well as varying the footpoint magnetic latitude error, affects the occurrence and quality of conjunctions. Although we did not conduct a study on the error in the location, we hope that the quality indicator will help researches determine when to be more cautious when studying conjunctions.

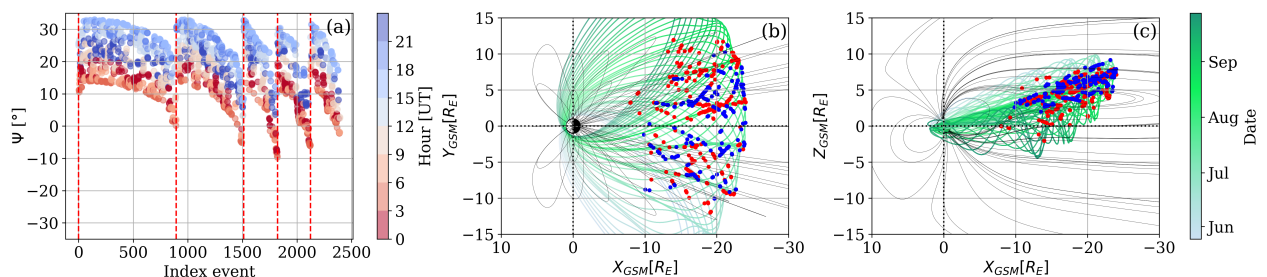


**Fig. 1.** Observational bias of Earthward BBFs events related to the MMS tail/summer season. (a) Tilt angle at the moment of the 2135 BBF event chronologically ordered. The dashed red lines correspond to the dates of the first BBF detected during each MMS tail summer season: 2017-05-16, 2018-05-30, 2019-06-18, 2020-06-27, and 2021-06-26. (b-c) BBF position in GSM coordinates for the BBF event detected during the second MMS tail season (red and blue dots) and when  $20^\circ < \Psi < 30^\circ$  (blue dots). The background magnetic field lines are produced with T89 for  $\Psi = 25^\circ$ ,  $K_p=1$ ,  $V_{x,GSE} = -400$  km/s.

## 2. Data and Models

### 2.1. The BBF database

We used the BBF database developed by [Richard et al. \(2022b\)](#) which consists of the initial and end time of 2394 BBFs detected in the magnetotail by MMS 1 during the five magnetotail seasons between 2017-2021. A full description of the selection criteria can be found in [Richard et al. \(2022a\)](#).

Since our goal is to find the ground footpoint of the BBFs, we have restricted our database to Earthward-moving BBFs, which constitute 89% of the total database. The mean and median duration of these Earthward BBFs are 3.60 minutes and 2.63 minutes, respectively, with approximately 80% of the events lasting less than 5 minutes. After excluding an outlier with a duration of  $\approx 3$  hours, the BBF dataset consists of 2135 events, with the longest event lasting 35 minutes.

Due to the MMS orbit, there is an observational bias in the detected BBFs, as illustrated in Figure 1. The first panel shows that the tilt angle ( $\Psi$ ) at the moment of the BBF detection is predominantly positive (mean  $\Psi = 18^\circ$ ), peaking in June and gradually decreasing toward the end of the MMS tail season. Superimposed on this annual variation is the daily variation, with the largest  $\Psi$  values occurring between 15:00 and 18:00 UT (Figure 1a).

Additionally, Figure 1b-c shows the MMS orbit for the second MMS season (2018-05-25 to 2018-09-28) and the BBFs detected during the same period (blue dots correspond BBF detected when  $20^\circ < \Psi < 30^\circ$ ). In the  $Y_{GSM}$  coordinate, the MMS apogee begins the magnetotail season at  $Y_{GSM} < 0$ , shifting to  $Y_{GSM} > 0$  by the end of the season. Similarly, the apogee in  $Z_{GSM}$  starts positive and transitions to negative as the season progresses, in line with the tilt angle.

### 2.2. Solar wind and ground magnetic conditions

For determining the footpoints, it is necessary to incorporate data on solar wind and geomagnetic conditions. We used 1-minute resolution solar wind parameters, including solar wind dynamic pressure ( $P_{dyn}$ ), interplanetary magnetic field (IMF), and solar wind velocity in GSE co-

**Table 1.**  $P_{dyn}$ : the dynamic pressure of the solar wind;  $B_{y,IMF}$  and  $B_{z,IMF}$ : y and z components of the IMF.  $r_{GEO}$ : geocentric distance

| Model | Inputs  | Valid region          |
|-------|---|-----------------------|
| T89   | Kp  | $r_{GEO} \leq 70R_E$  |
| T96   | $-100 < Dst < 20$ nT, $0.5 \leq P_{dyn} \leq 10$ nPa,<br>$ B_{y,IMF}  \leq 10$ nT, $ B_{z,IMF}  \leq 10$ nT | $r_{GEO} \leq 60R_E$  |
| T01   | Dst, $P_{dyn}$ , $B_{y,IMF}$ , $B_{z,IMF}$ , $G_1$ , $G_2$  | $X_{GSM} \geq -15R_E$ |
| T04   | Dst, $P_{dyn}$ , $B_{y,IMF}$ , $B_{z,IMF}$ , $W_1$ to $W_6$   | $X_{GSM} \geq -15R_E$ |

ordinates ( $V_i$ ), sourced from OMNIweb <https://omniweb.gsfc.nasa.gov/>. The geomagnetic Dst index was replaced by the higher resolution Sym-h index, and the Kp index was replaced by the higher resolution Hp030 index (Yamazaki et al., 2022). Additionally, the solar wind driving parameters  $G$  and  $W$  (Qin et al., 2007) were obtained from the SpacePy Python package <https://spacepy.github.io/index.html>.

The solar wind conditions for each event were determined by calculating the mean values within a 30 minutes window centered on each BBF event. Events lacking solar wind data within this time window were excluded from the analysis, as this data is necessary for running the mapping models. Consequently, the BBFs database was reduced to 2079 BBF events.

The geomagnetic conditions during the BBFs events are characterized by a mean Sym-h index of  $-10$  nT and median of  $-8$  nT. Notably, 72% of the events have Sym-h values between  $-30$  nT and  $0$  nT, which is above the threshold typically associated with weak geomagnetic activity. This is consistent with the distribution of the Hpo30 index, where 78% of events have Hpo30  $< 3$ .

### 2.3. Mapping models

The footpoints for each of the 2079 BBF events were computed using the Tsyganenko models T89, T96, T01, and T04, available through the Geopack Python library (<https://github.com/tsssss/geopack>). Each model requires the event date and solar wind velocity to calculate the dipole tilt angle. The input parameters and valid regions for each model are summarized in Table 1.

In the case of T01 and T04 these models are only valid sunward of  $X_{GSM} = -15 R_E$ . Consequently, only 12.5% of the 2079 BBF events satisfy this criterion and can be mapped to the Earth's surface. Additionally, after visually inspecting the traced field lines, two criteria were applied to exclude events that could not be accurately modeled (see examples in Appendix A). The behavior of the models for such excluded events are beyond the scope of this work. The two criteria that were used to retain valid events are as follows:

1. The footpoint in the north and south hemisphere reaches the Earth's surface.
2. The magnetic field line goes out and returns only once, making a single loop.

The database of 2079 BBF events with the Tsyganenko input and the footpoint output for each T89, T96, T01 and T04 model are available at Lanabere et al. (2024).



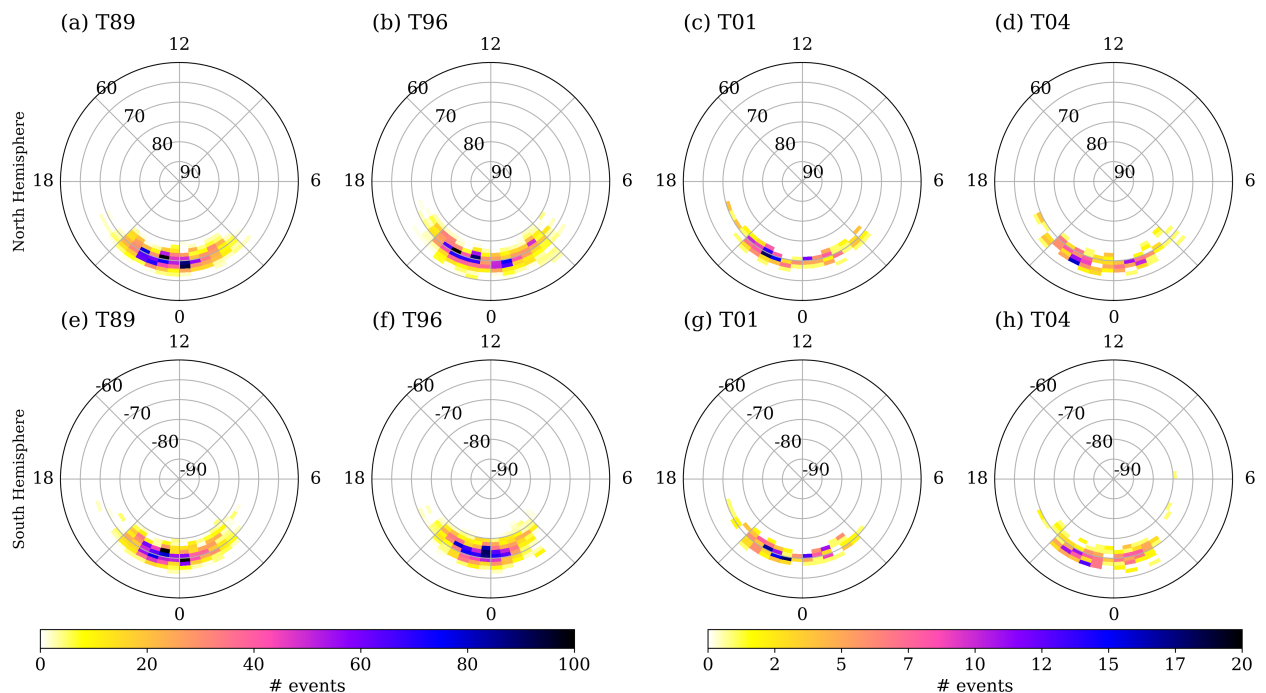


**Fig. 2.** footpoint histogram in MLAT and MLT (AACGM coordinates) of BBF in north and south hemisphere for different Tsyganenko models. Bin size:  $1^\circ \times 0.5$  hour. Altitude of footpoint is 462 km.

### 3. BBF footpoints from Different Tsyganenko Models

We analyzed the footpoint of the BBF events in both the Northern hemisphere and Southern hemisphere (NH and SH respectively) for each Tsyganenko model. The footpoint is presented in magnetic latitude (MLAT) and magnetic local time (MLT) in the altitude adjusted corrected geomagnetic (AACGM) coordinates. The altitude of the BBF footpoint is set at 462 km, which corresponds to the altitude of the Swarm satellites A and C.

#### 3.1. Statistical Footpoint Positions for Each Tsyganenko Model

The footpoint histogram for each Tsyganenko model is shown in Figure 2. Statistically, the footpoints appear similar across all the mapping models, suggesting that despite the inherent differences in how these models represent Earth's magnetosphere, they statistically converge on a similar spatial distribution of BBFs.

The magnetic latitude (MLAT) footpoints of BBFs are generally concentrated around  $70^\circ \pm 4^\circ$  in both hemispheres. The slight spread in MLAT could be indicative of variations in geomagnetic conditions or differences in the way each Tsyganenko model maps to the ionosphere. In terms of magnetic local time (MLT), BBFs predominantly have their ionospheric footpoints around midnight  $\pm 3$  hours, with a clear peak in the pre-midnight sector primarily associated with substorm onsets.

While the statistical distribution of BBF footpoints is similar across Tsyganenko models, significant variations can occur for specific events. These differences are crucial when searching for

conjunctions. To better understand these discrepancies, we perform a comparative analysis of the footpoint locations produced by each Tsyganenko model, using the T89 model as the reference. T89 was chosen as the benchmark because it maps the largest number of BBFs, thanks to its broader inclusion criteria and fewer restrictions on input parameters

### 3.2. Comparison of BBF Footpoints: T89 vs. Later Models

Figure 3(a-f) presents the MLT footpoint positions for each hemisphere, comparing the T89 model with T96, T01, and T04 models. Additionally, the mean bias error (MBE) and root mean square error (RMSE) are included to quantify the differences between the models.

The MLT position between the models is quite similar, with differences typically within  $\pm 1$ MLT. However, from Figure 3a,d we notice that in the northern hemisphere, T96 tends to shift footpoints towards later MLT in the post-midnight sector and earlier MLT in the pre-midnight sector. In contrast, the southern hemisphere shows the opposite behavior. The largest MLT differences are observed between T89 and T04 in the south hemisphere.

The MLAT footpoint position is shown in Figure 3(g-l) together with the MBE and RMSE. Compared to the MLT coordinate, MLAT differences between models are more pronounced. For instance, the MBE between T89 and T96 is  $MBE = 0.22^\circ$  and  $MBE = 0.81^\circ$  for north and south hemispheres respectively. This suggests that MLAT positions calculated using T96 are, on average, closer to the pole than those from T89. A similar trend, but with larger MBE values ( $MBE = 1.18^\circ$  and  $MBE = 1.14^\circ$  for north and south hemispheres), is observed between T89 and T01.

### 3.3. Relation Between Footpoint Positions and Input Parameters

In terms of MLT, the strongest correlation was observed with the BBF's  $Y_{GSM}$  position (see Figure 4), with Pearson correlation coefficients around  $-0.9$  in all cases. As expected, the linear coefficients indicate that on average pre-midnight events are associated with  $Y_{GSM} > 0$ , while post-midnight events correspond to  $Y_{GSM} < 0$ . Additionally, models that use  $B_{y,IMF}$ ,  $B_{z,IMF}$  as input parameters show a relation between MLT and the IMF clock angle ( $\theta_c = \text{atan}(B_y/B_z)$ ). For instance, in the northern hemisphere if  $\theta_c \approx 90^\circ$  ( $B_{y,GSM} > 0$ , pointing towards dusk) the MLT is earlier compared to  $\theta_c \approx 270^\circ$  ( $B_{y,GSM} < 0$ , pointing towards dawn). An opposite behavior is observed in southern hemisphere.

The relationship between MLAT and the input parameters of the models is more complex. As expected, cross-correlation analysis between the input variables and MLAT reveals a moderate correlation with the distance of the BBF from Earth, indicating that the MLAT shifts closer to the pole as the distance from Earth increases. Other parameters that influence MLAT vary depending on the specific model used. The Pearson and Spearman correlation coefficients for each model and hemisphere are presented in Figure 5.

For the simplest model (T89), BBFs detected at similar distances from Earth exhibit footpoints that reach lower magnetic latitudes as Hp030 values increase. A similar behavior is observed with T96 but with the coupling function  $E_{KLV} = V^{4/3} B_T \sin^2(\theta_c/2) p^{1/6}$  proposed by Vasyliunas et al. (1982). This coupling function relates all the solar wind input parameters and presents larger correlation than the Sym-h index ( $r_p = -0.18$  and  $r_s = -0.08$ ). In the case of T01, the correlation with distance is more evident but no relation with input parameters was found maybe due to the low number of events. Finally, T04 presents six input parameters that estimate the exchange of energy

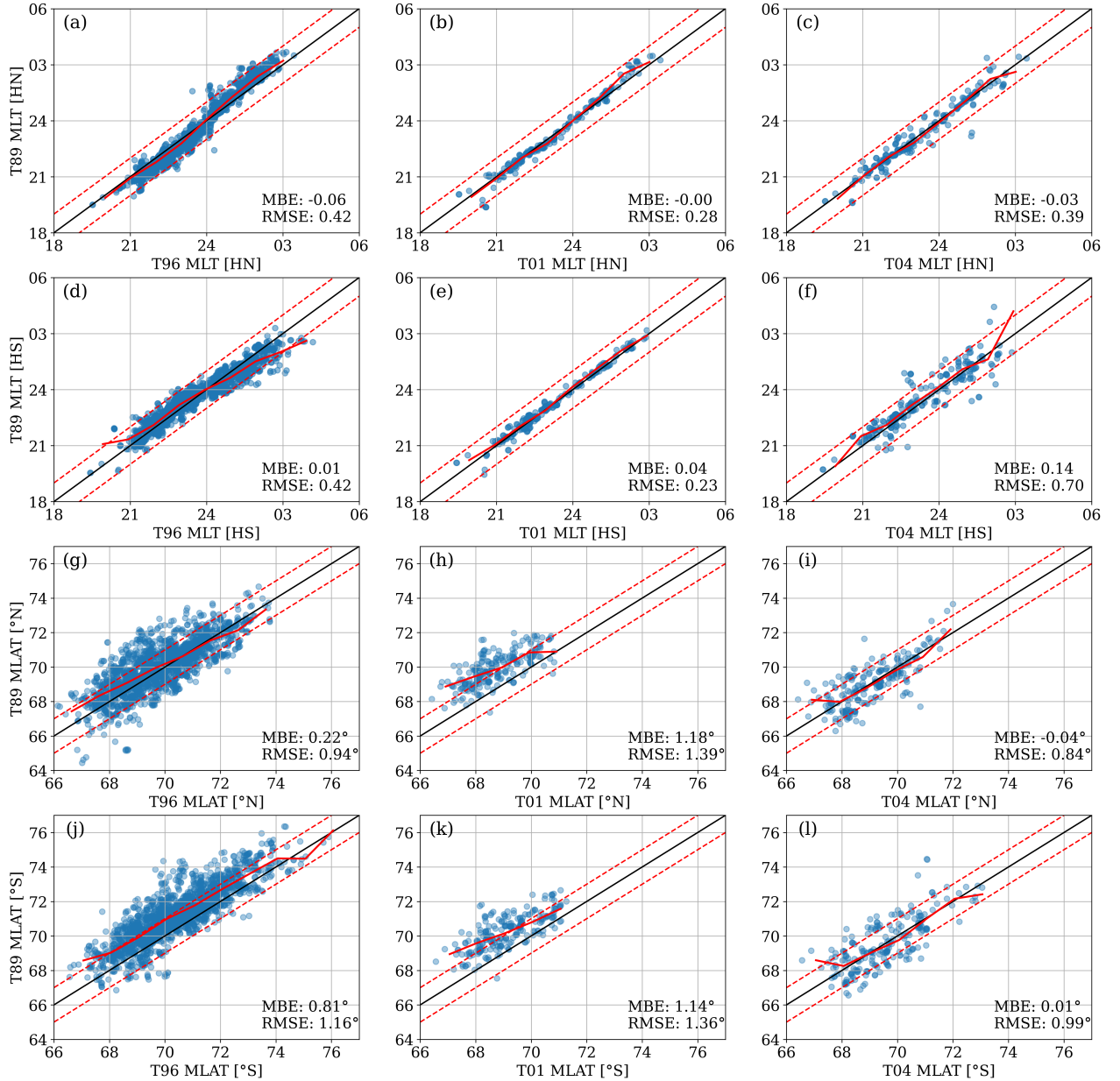


**Fig. 3.** Comparison of footpoint position in AACGM coordinates for T89 versus the T96, T01, and T04. (a-f) Magnetic local time (MLT). (g-l) Magnetic Latitude (MLAT). The diagonal line represents the ideal scenario where both models agree perfectly. The dashed red lines indicate a difference of  $\pm 1$  (hour for the MLT plots and degrees for MLAT plots) from the ideal scenario. The solid red line represents the mean value. For each plot the mean bias error (MBE) and the root mean square error (RMSE) are indicated.

from the interplanetary medium to the magnetosphere, the parameter with the largest correlation was  $W_1$  (see [Qin et al. \(2007\)](#) for the derivation of the parameter).

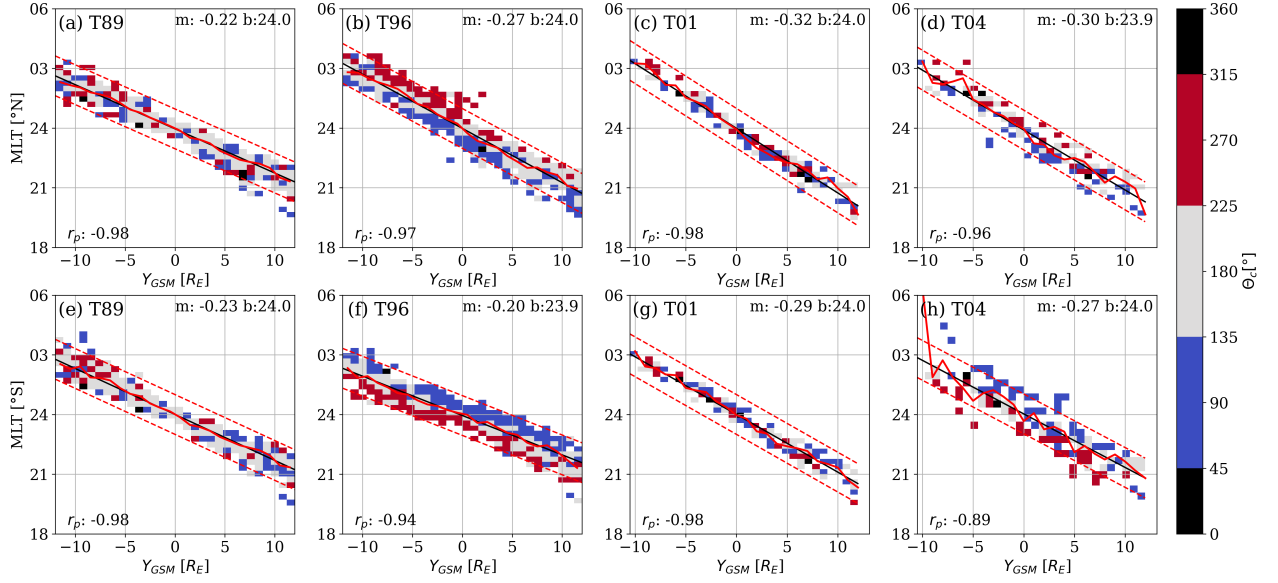


**Fig. 4.** Relation between the BBF position ( $Y_{\text{GSM}}$ ) and MLT for each Tsyganenko model. The solid black line is the linear regression. The dashed red line is the linear regression shifted  $\pm 1$  hour. The solid red line corresponds to the mean value.

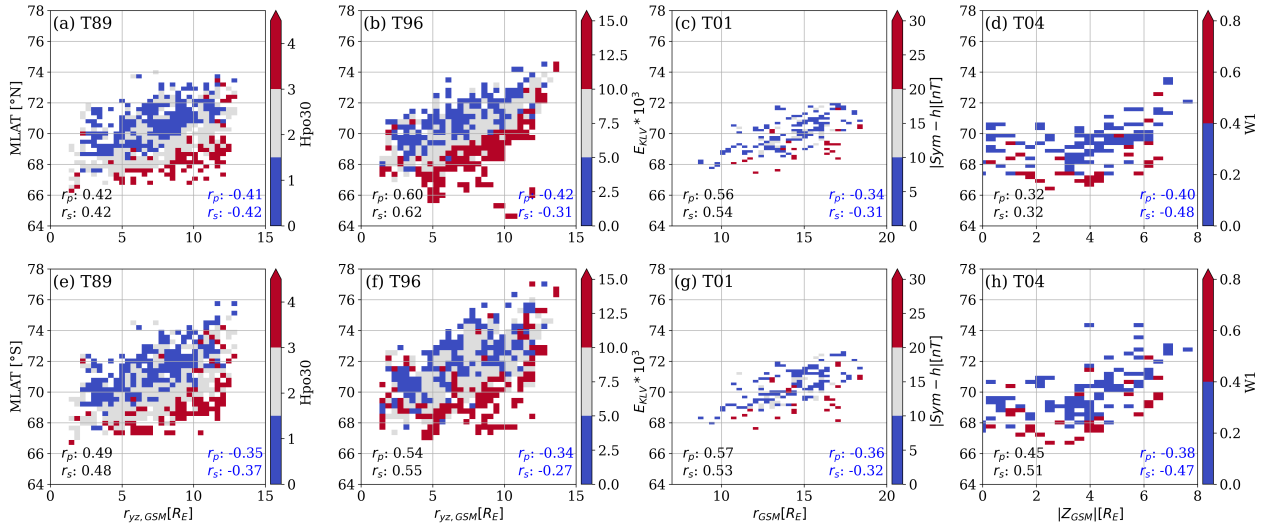


**Fig. 5.** Relation between the BBF distance to Earth and MLAT for each Tsyganenko model. The color scale indicate the input variable or derived variable from the input parameters, with the largest correlation with MLAT.

### 3.4. Analysis of Model Differences Based on Input Parameters

The MLT difference between T89 and (T96, T01 and T04) as a function of  $Y_{\text{GSM}}$  and clock angle  $\theta_c$  are shown in Figure 6. In the northern hemisphere, the T89 model tends to display footpoints closer to midnight compared to T96, while the opposite is observed in the southern hemisphere. This behavior is not observed when comparing to the other models (T01 and T04). The analysis of

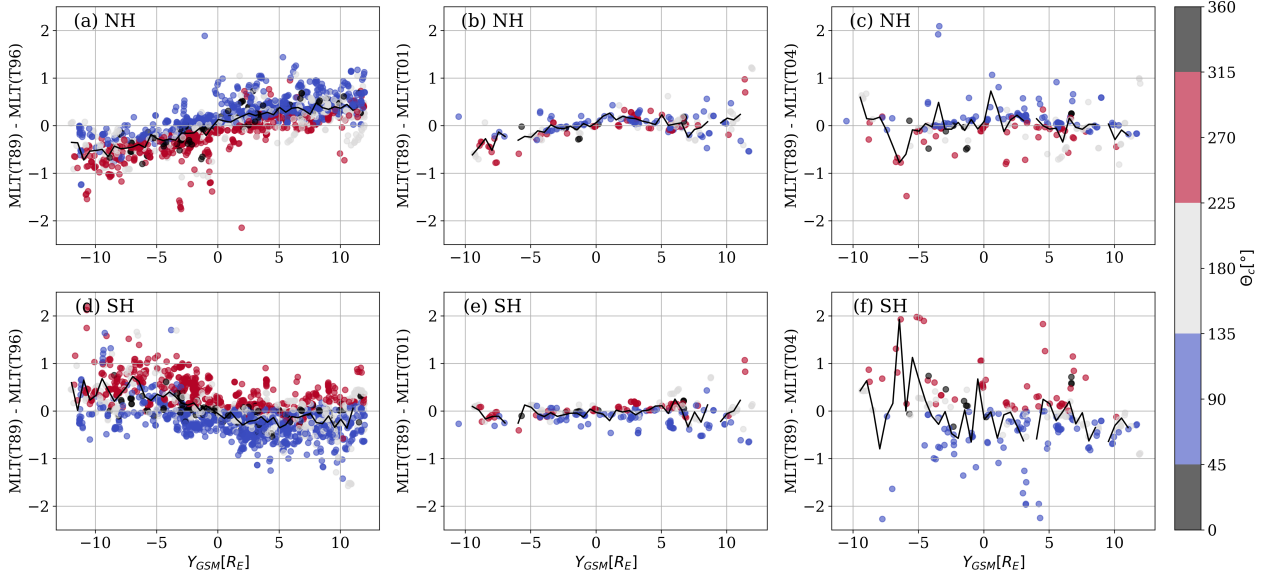


**Fig. 6.** Difference between T89 and (T96, T01 and T04) against the  $Y_{\text{GSM}}$  position of the BBF. The color scale is interplanetary magnetic field clock angle ( $\theta_c$ ) and the solid black line is the mean value.

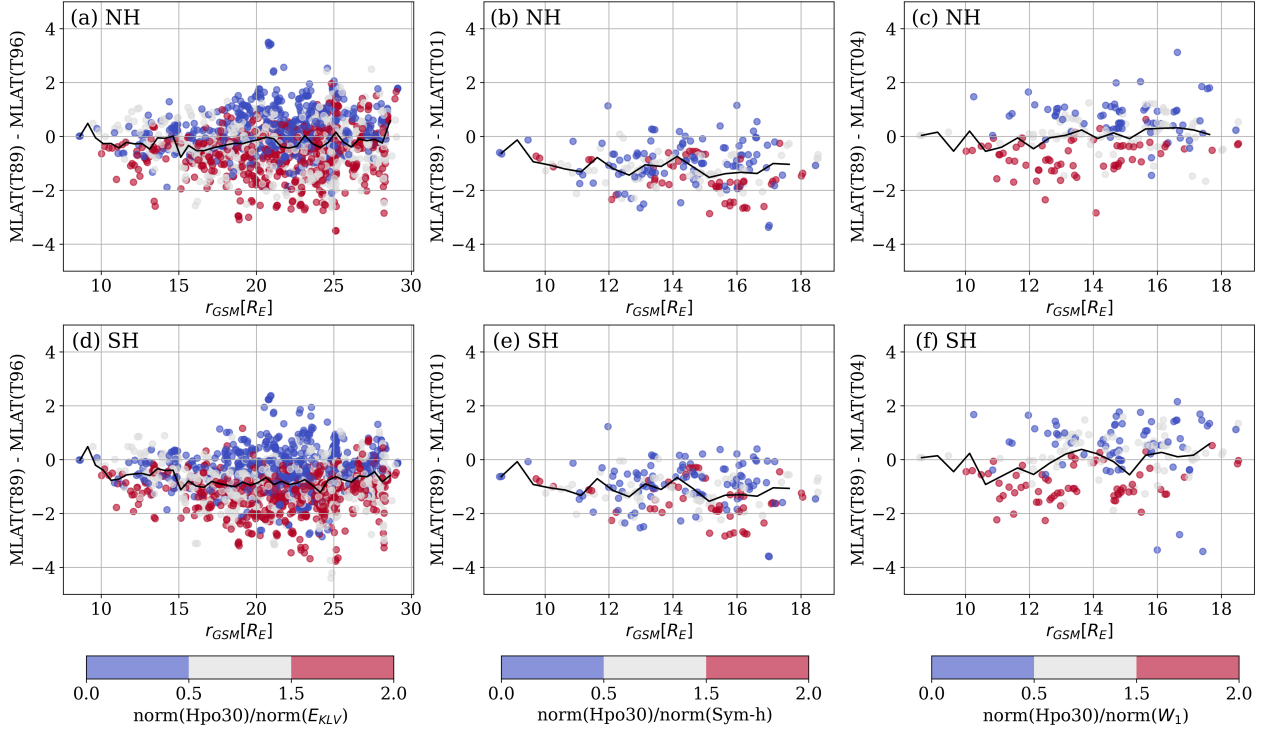
the clock angle dispersion around the mean error shows that when  $\theta_c = 90^\circ$  (blue dots) the MLT is later for T89 than T96, and earlier for  $\theta_c = 270^\circ$  (red dots). An opposite behavior is observed in the southern hemisphere. Despite the low statistics, similar trends are observed in the comparison between T89 and (T01, T04).

Figure 7 shows the difference between T89 and (T96, T01 and T04) as a function of the distance of the BBF from Earth and the relative magnitudes of the proxies for Earth’s magnetospheric dynamics. This ratio indicates how the input parameter for T89, as represented by Hpo30, relates to  $E_{\text{KLV}}$ , Sym-h, and  $W_1$  for models T96, T01 and T04, respectively, after normalizing by their median values. In the northern hemisphere, for BBFs located at the same  $r_{\text{GSM}}$ , when Hpo30 is greater than  $E_{\text{KLV}}$  (red dots), T89 footpoints are at lower latitudes compared to T96 (Figure 7a). Conversely, when  $E_{\text{KLV}}$  is greater than Hpo30 (blue dots) T89 footpoints are closer to the pole than the ones computed with T96. The same behavior is observed in the southern hemisphere Figure 7d. A similar trend is observed when comparing T89 with T04, although it is less apparent with T01, possibly due to lower statistics.

### 3.5. Footpoint Proximity as a Measure of Mapping Quality

The difference between the footpoints computed using the T89 and T96 models (Figure 6a,d and Figure 7a,d) shows that more than 90% percent of the BBF footpoints in both hemispheres have an absolute MLT error less than 1 hour and an absolute MLAT error less than  $2^\circ$ . At latitude of  $70^\circ$ , these correspond to a east-west extent of approximately 568 km and a north-south extent of 222.64 km, respectively. These differences are significantly larger than the estimated mapped mean dimensions of dipolarization flux bundles (DFBs), which are often found within BBFs. According to Engebretson et al. (2024), a DFB with mean radius of  $0.9R_E$  (Liu et al., 2013) mapped to the





**Fig. 7.** Difference between T89 and (T96, T01 and T04) against the  $r_{\text{GSM}}$  position of the BBF. The color scale represents the ratio of the normalized Hpo30 geomagnetic index (input parameter in T89) to the normalized input parameters with the highest correlation ( $E_{\text{KLV}}$ , Sym-h, and  $W_1$  for T96, T01, and T04 respectively). The solid black line indicates the mean value. Normalization was performed using the median value.

ionosphere, has an east-west extent of approximately 180 km (0.3 MLT at  $70^\circ\text{N}$ ) and a north-south extent of about 90 km ( $0.81^\circ$ ). This is consistent with our estimation of BBF footprint size, detailed in Appendix B. Assuming a dipole field model and a circular cross section, we calculated a BBF cross-section in the ionosphere of approximately  $110 \text{ km} \pm 30 \text{ km}$ .

Due to both statistical and physical considerations of the footprint distances, we used two different criteria to assign a quality metric to the mapping. Based on the statistical difference between footpoints calculated with T89 and T96 models, we define a maximum distance between footpoints of  $\pm 1$  hour in MLT and  $\pm 2^\circ$  in MLAT. Meanwhile, considering the physical size of the footprint, the maximum distance is 0.3 MLT and  $0.81^\circ$ . We introduce a footprint quality metric ( $Q_{fp}$ ) for each BBF mapped event, where  $Q_{fp} = 1$  if the footprint distances between T89 and T96 fall within both coordinate error ranges,  $Q_{fp} = 2$  if only one coordinate falls within the range, and  $Q_{fp} = 3$  if the footpoints are separated by distances greater than these ranges. In the first case this fraction of  $Q_{fp} = 1, 2,$  and  $3$  respectively are 94%, 5.3% and 0.7% for the Northern hemisphere, and 89.85%, 10.14% and 0.05% for the Southern hemisphere. In the second case, where the BBF footprint size is considered, the results are 63.5%, 35.2% and 1.3% for the Northern hemisphere, and 46.3%, 53.1% and 0.6% for the Southern hemisphere, for  $Q_{fp} = 1, 2,$  and  $3$  respectively.

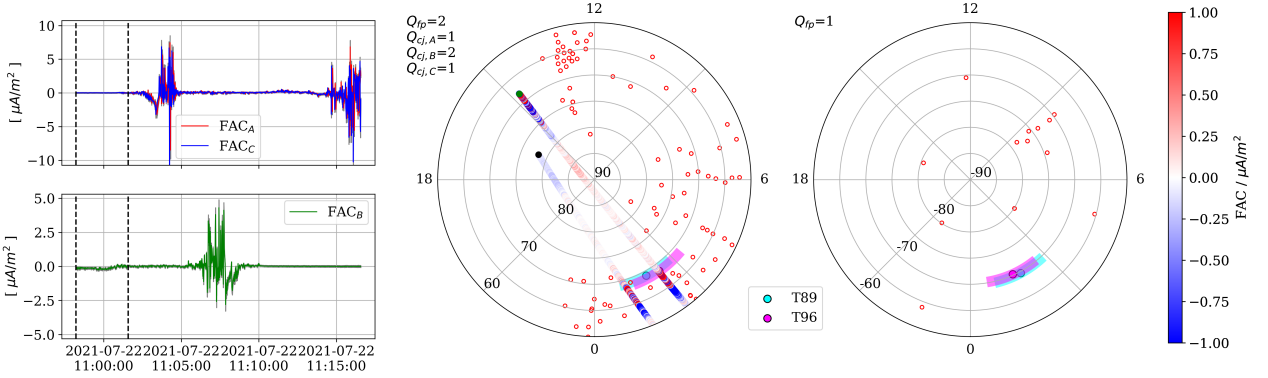


**Fig. 8.** Example of BBF footpoint-Swarm conjunction for Swarm trace  $\Delta t = 15$  minutes after end time of BBF detection. (Left) Swarm A, B and C FAC measurements, and the BBF duration indicated with the two vertical dashed lines. (Right) Polar plot with Swarm traces across the North and South hemispheres and the corresponding FAC intensity. The BBF footpoint for the different Tsyganenko models are represented by circles, with shaded areas indicating the errors  $Err_{MLAT} = \pm 1^\circ$ ,  $Err_{MLT} = \pm 1$ . The  $Q_{fp}$  and  $Q_{cj}$  indicate the footpoint quality and conjunction quality with Swarm A, B, and C.

#### 4. BBF and Swarm conjunctions

In the previous section, we observed that the BBF footpoint locations predicted by different Tsyganenko models exhibit variations and that these discrepancies are influenced by geomagnetic conditions and the specific position where the BBF was detected. Consequently, defining conjunctions can be challenging due to these variations in model predictions. In this section we want to implement the analysis we have discussed to investigate the impact on MMS-Swarm BBF conjunctions.

To address this, we will analyze how the number of detected conjunctions changes with different definitions of conjunction criteria. Specifically, we will investigate the impact of varying the MLAT error ( $Err_{MLAT}$ ) and the time interval between the detection of BBFs and the Swarm satellites' path ( $\Delta t$ ). The MLT error is set at  $\pm 1$  hour because it correspond to the typical dispersion of BBF footpoints for different solar wind and magnetospheric conditions. This analysis aims to quantify how adjustments in these parameters influence the identification of conjunctions.

We consider a conjunction if at least one footpoint with its error coincides with the Swarm trace. To evaluate the quality of these conjunctions, we define a conjunction quality metric ( $Q_{cj}$ ). The metric is defined as follows: if the Swarm trace passes through both footpoints, the conjunction is assigned a quality of  $Q_{cj} = 1$ ; if the Swarm trace intersects only one footpoint, it is assigned a quality of  $Q_{cj} = 2$ . The footpoint in AACGM is calculated at altitude 462 km for Swarm A and C, and 510 km for Swarm B. Figure 8 shows an example of Swarm A, B and C traces during  $\Delta t = 15$  minutes, across the south and north hemispheres, the corresponding FAC magnitude, and the BBF footpoint with the different Tsyganenko models. The shaded area of the footpoint is given by  $Err_{MLAT} = \pm 1^\circ$ , and  $Err_{MLT} = \pm 1$  hour. In this case we detect a conjunction in the southern hemisphere with Swarm B.

Figure 9 displays the number of Swarm-BBF footpoint conjunctions in the northern hemisphere and the fraction of  $Q_1$  (i.e.,  $Q_{fp} = 1$  and  $Q_{cj} = 1$ , indicating closely footpoints computed with the T89 and T96 models and Swarm satellite passing through both footpoints) for two different criteria. The range for  $\Delta t$  is estimated from the BBF database by assuming that the FACs are carried by Alfvén waves (Keiling, 2009). The median length of the magnetic field line from the BBF position to the northward ionospheric footpoint is  $25 R_E$ , and the median Alfvén velocity of BBFs is  $470 \text{ km s}^{-1}$ . Assuming that the velocity is constant, the median time delay is  $\Delta t = 6 \text{ min}$ . When considering the 10th and 90th percentiles of the field line length and Alfvén velocity the extreme  $\Delta t$  values are 1.9 and 24.5 minutes. The latitude range was selected up to  $\pm 5^\circ$ , which corresponds to a distance comparable to 1 hour MLT.

The results reveal that Swarm B shows a greater number of conjunctions compared to Swarm A and C. As expected, the number of conjunctions increases when increasing MLAT and time interval. In general, extending the time window by 1 minute leads to a more number of conjunctions than adjusting the MLAT error by  $\pm 0.5^\circ$ . From the two lower panels, we see that the fraction of  $Q = 1$  conjunctions with Swarm B is more homogeneous than Swarm A and C, which present a clear region of low fraction of  $Q = 1$  around ( $\Delta t = [0, 6]$  minutes and  $Err_{MLAT}$  around  $3^\circ\text{N}$ ). When considering the BBF footprint size, we notice that in all cases less than half of the total number of conjunctions present  $Q = 1$ . This highlight the challenges in achieving precise spatial alignment between BBF footpoints and satellite traces. Depending on the aim of the research, different approaches may be appropriate for selecting conjunctions. If one is interested in detailed case studies, it is possible to work with very close conjunctions. However, if the goal is to conduct a statistical study, increasing the allowed MLAT error and extending the time window may be necessary to capture a broader range of conjunctions.

## 5. Discussion

Utilizing a database of 2394 busy bulk flows detected by MMS and applying four different Tsyganenko models, we mapped the BBFs to the Earth’s ionosphere. On average BBF footpoints are located in MLT coordinates around midnight, with a range of  $\pm 3$  hours, peaking in the pre-midnight sector (Figure 2). This location aligns with regions of intense geomagnetic activity, likely associated with the substorm activity Weigel et al. (2002).

The magnetic latitude of BBF footpoints are generally concentrated around  $70^\circ \pm 4^\circ$  in both hemispheres. The Tsyganenko model T96 and T01, on average, returns a footpoint closer to the pole compared to T89. This difference could be attributed to a less stretched magnetotail in T01 and T96, as suggested by the traced field lines of the mapped BBFs (not shown). Similarly, Peredo et al. (1993) reported that the T89 model is known for excessively stretching the magnetotail in the region  $-10R_E < X_{GSM} < -22R_E$ .

The MLT position of the footpoints exhibits a linear relationship with the  $Y_{GSM}$  position of the BBF, intersection MLT=0 at  $Y_{GSM} = 0$ . This means that on average field lines represented by the Tsyganenko models do not cross the midnight meridian. Additionally, all Tsyganenko models that uses  $B_y$  and  $B_z$  as input parameters (T96, T01, and T04) show a correlation with the IMF clock angle. For instance, figure 4 shows in the northern hemisphere that the linear regression shifts toward later MLT when  $\theta_c \approx 270^\circ$  and earlier for  $\theta_c \approx 90^\circ$ . An opposite behavior is observed in the southern hemisphere.

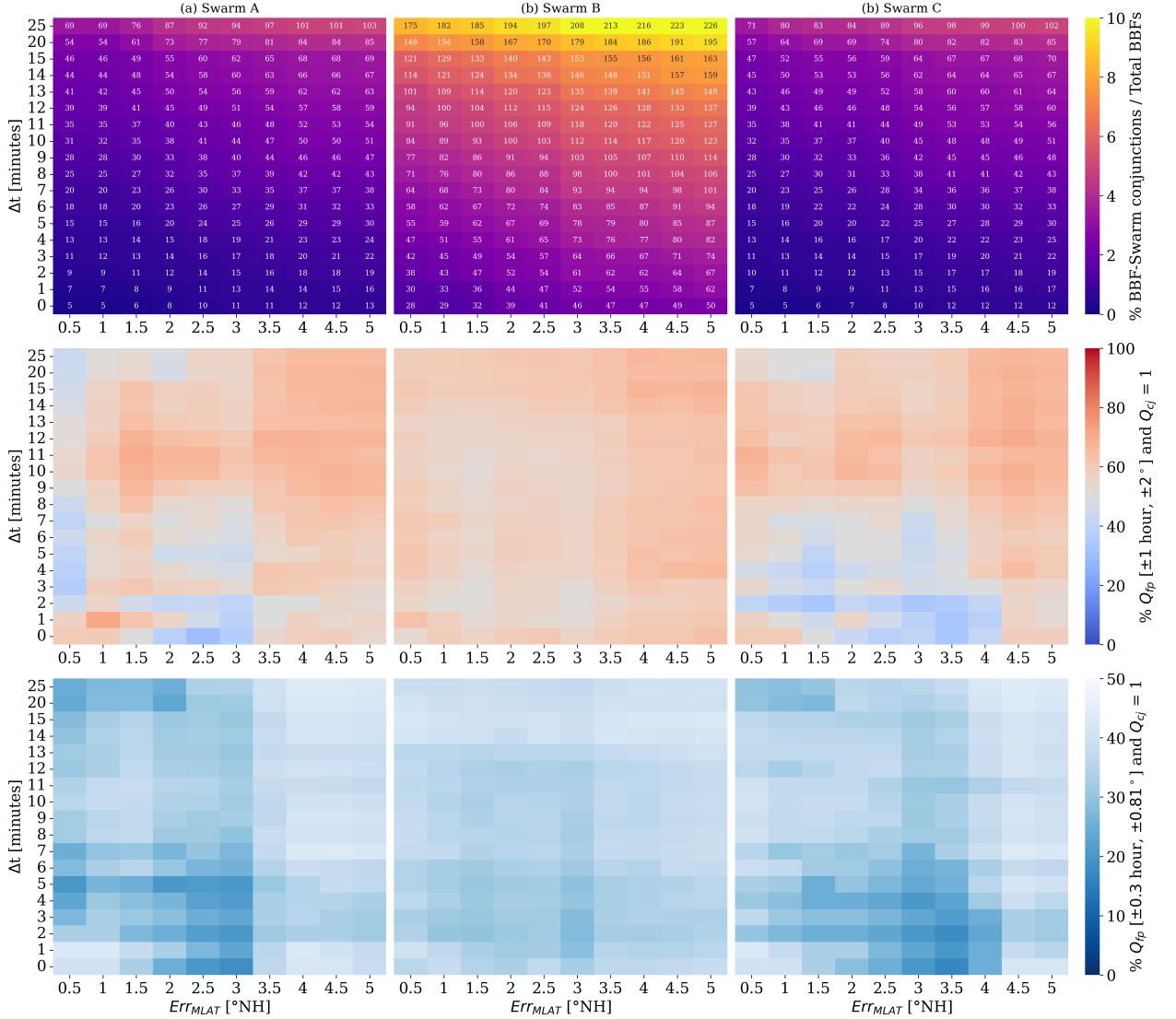


**Fig. 9.** First row: Number of BBF footpoint-Swarm conjunctions for different time and MLAT position error ( $\Delta t$ ,  $\pm Err_{MLAT}$  respectively) for the Northern hemisphere and each Swarm satellite. The number inside each bin is the total number of conjunctions and the color is the percentage with respect to the total number of BBFs. Second row: Percentage of conjunctions with  $Q_{fp} = 1$  (the footpoint distance computed with T89 and T96 models is lower  $\pm 1$  hour in MLT and  $\pm 2^\circ$  in MLAT) and  $Q_{cj} = 1$  (Swarm satellite passing through both footpoints). Third row: Similar to second row but with  $Q_{fp} = 1$  (the footpoint distance computed with T89 and T96 models is lower  $\pm 0.3$  hour in MLT and  $\pm 0.81^\circ$  in MLAT). Column (a) BBF conjunctions with Swarm A. Column (b) BBF conjunctions with Swarm B. Column (c) BBF conjunctions with Swarm C.

The MLAT position is influenced by both the distance to Earth and the input parameter representing magnetospheric dynamics. As expected, more distant BBFs map, on average, to higher latitudes. Additionally, higher values of the magnetospheric dynamics parameter correspond to lower latitudes for the footpoints. This pattern aligns with the equatorward shift of the low-latitude boundary

of the auroral oval during the growth phase of a substorm [Akasofu \(2017\)](#). However, the parameters used to model magnetospheric dynamics differ across the various Tsyganenko models, leading to discrepancies in the latitude of the footpoints when one parameter indicates higher magnetospheric activity than another. Interestingly, T96 shows a low correlation with the Sym-h index ( $r_p = -0.18$  and  $r_s = -0.08$ ). This is likely because, during BBF events, the Sym-h index typically reflects non-storm periods ( $-30 < \text{Sym} - h < 0$  nT).

The relation of BBF-footpoints against the dipole tilt angle could not be explored in this work with the actual database. This should be taken into account when analyzing ionosphere and ground signatures. According to [Eggington et al. \(2020\)](#), the tilt angle has a strong effect on the location and intensity of magnetic reconnection which map down to the ionosphere. For instance, the polar cap contracts as the tilt angle increases, and FACs migrate to higher latitudes, exhibiting changes in morphology. To reduce the detection bias introduced by orbital effects, incorporating BBFs detected by other spacecraft, such as THEMIS and CLUSTER, can provide a more comprehensive and unbiased analysis ([Runov et al., 2009](#); [Cao et al., 2006](#)).

## 6. Conclusion

In this paper we provided an analysis of the variability in BBFs footpoint using four different Tsyganenko models and its impact on the number of BBF-Swarm conjunctions, with the following results:

- Bursty bulk flows footpoints in the ionosphere are 90% of cases concentrated around  $70^\circ \pm 4^\circ$  (MLAT) and around 0 MLT  $\pm 3$  hours, with a peak in the pre-midnight sector.
- As expected, the BBF footpoint position in MLAT coordinate is closer to the pole as the BBF distance from Earth increases and closer to the equator for larger magnitudes of the Tsyganenko input parameter that quantifies the magnetospheric current systems (i.e, Kp, Dst,  $E_{kv}$ ,  $W_1$  for T89, T96, T01 and T04 respectively).
- MLAT difference between models shows footpoints closer to the pole for models T96, T01 respect T89. This is related to the excessively stretched magnetotail in model T89.
- footpoints of BBFs located at similar geocentric distances are found at lower MLAT for the model with the higher relative magnitude of the input parameter (Kp, Dst,  $E_{kv}$ ,  $W_1$  for T89, T96, T01 and T04 respectively) when both are normalized.
- The difference between the footpoints computed with the T89 and T96 models are within the range of MLAT  $\pm 2^\circ$ , based on the 90th percentile of the data.
- BBF footpoint position in MLT coordinate is strongly correlated with the  $Y_{\text{GSM}}$  position of the BBF and the interplanetary magnetic field clock angle.
- The MLT differences between the models are within the range of  $\pm 1$  hour, based on the 90th percentile of the data. The footpoints of the T96, T01 and T04 models at similar  $Y_{\text{GSM}}$  position are located at earlier MLTs compared to the T89 footpoint when the  $\theta_c \approx 270^\circ$ . In contrast they appear at later MLT when  $\theta_c \approx 90^\circ$ .



- Assuming that BBF-driven disturbances propagate along magnetic field lines at constant Alfvén velocity, and using the median length of the field line to the northward ionospheric footpoint  $L = 25R_E$ , the median traveling time is  $\Delta t = 6$  min. When considering the 10th and 90th percentiles of the field line length and Alfvén velocity the extreme  $\Delta t$  values are 1.9 and 24.5 minutes.
- The number of BBF-Swarm conjunctions is larger with Swarm B than Swarm A/C. Moreover, Swarm B presents, on average, more conjunctions where the footpoints distance is lower than ( $\pm 0.3$  hours in MLT and  $\pm 0.81^\circ$  in MLAT) and Swarm path goes through both footpoints.

*Acknowledgements.* This work was supported by the ESA 4D ionosphere initiative. ESA contract No. 4000143412/23/I-EB

## Appendix A: Application of criteria to magnetic field line mapping

In some cases, the footpoints obtained from the Tsyganenko model may be unreliable. Here, we present three different scenarios of field line tracing to illustrate this. In Figure A.1a, all four Tsyganenko models (ie., T89, 96, T01 and T04) present both footpoints at the Earth’s surface and the field line makes a single loop. Figure A.1b presents both footpoints at the Earth’s surface but perform several loops. Finally, A.1c shows that the field line computed with T89 do not present a footpoint in the southern hemisphere.

## Appendix B: Estimate of the size of the footpoint

To obtain a physical size of the footpoint to look for conjunctions, we consider that the BBFs correspond to an individual flux tube/Dipolarizing Flux Bundle (DFB). From the conservation of magnetic flux along the DFB, we get  $A_1 B_1 = A_2 B_2$ , where  $A_1$ ,  $B_1$  and  $A_2$ ,  $B_2$  are the cross-sections of the DFB and magnetic field magnitudes at the BBF’s location and Swarm’s altitude, respectively. Assuming that the magnetic field at Swarm’s altitude follows a dipole field model, we obtain

$$A_2 = \frac{B_1}{B_0 r^{-3} \sqrt{1 + 3 \sin^2 \lambda}} A_1, \quad (\text{B.1})$$

where  $B_0 = 3.15 \times 10^4$  T the mean value of the magnetic field at the magnetic equator on the Earth’s surface,  $r = 1 + h/R_E$  with  $h = 465$  km the altitude of the footpoint region, and  $\lambda$  the magnetic latitude (MLAT). From MMS’s observations at the BBFs, we get  $B_1 = 12 \pm 7$  nT. From the mapping statistics (Figure 2), we have  $\lambda = 70^\circ \pm 4^\circ$ . Finally, assuming a circular cross section with radius  $R_1 \approx 2 R_E$  (Liu et al., 2015), we obtain  $R_2 \approx 110 \pm 30$  km.

## References

- Akasofu, S.-I., 2017. Auroral Substorms: Search for Processes Causing the Expansion Phase in Terms of the Electric Current Approach. *Space Sci Rev*, **212**(1-2), 341–381. 10.1007/s11214-017-0363-7. 5
- Angelopoulos, V., C. F. Kennel, F. V. Coroniti, R. Pellat, M. G. Kivelson, R. J. Walker, C. T. Russell, W. Baumjohann, W. C. Feldman, and J. T. Gosling, 1994. Statistical characteristics of bursty bulk flow events. *Journal of Geophysical Research*, **99**(A11), 21,257–21,280. 10.1029/94JA01263. 1

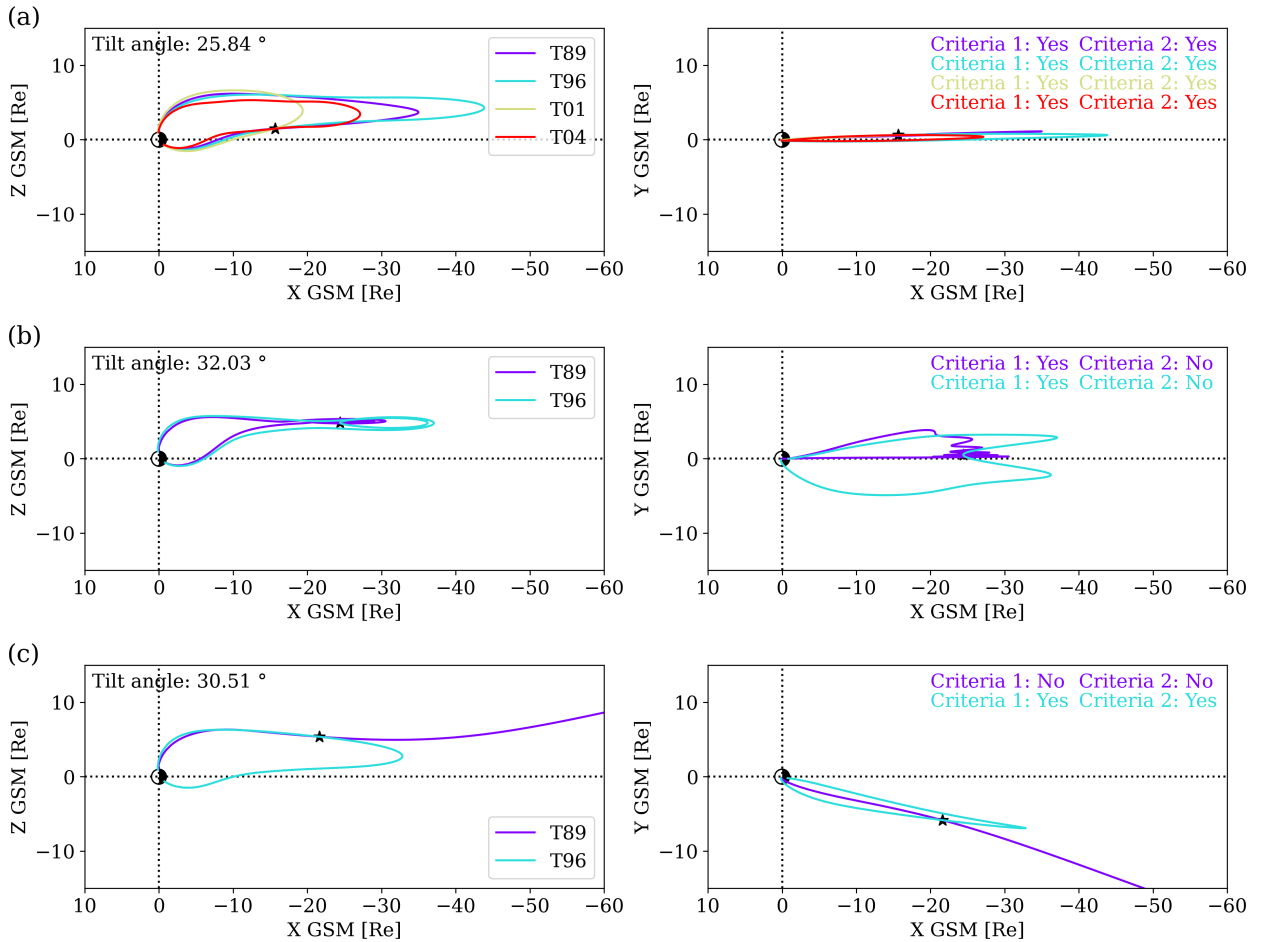


**Fig. A.1.** Example of three mapping scenarios when applying the Tsyganenko model to find the bursty bulk footpoint (indicated by an star). (a) The footpoint was calculated using four different Tsyganenko models, and all met both criteria. (b) Both Tsyganenko models (T89 and T96) returned both footpoints at the Earth’s surface, but the shape of the field line did not meet the second criterion (c) The footpoint computed with the T89 model did not return a footpoint in the southern hemisphere.

Aryan, H., J. Bortnik, J. Li, J. M. Weygand, X. Chu, and V. Angelopoulos, 2022. Multiple conjugate observations of magnetospheric fast flow bursts using THEMIS observations. *Annales Geophysicae*, **40**(4), 531–544. 10.5194/angeo-40-531-2022, URL <https://angeo.copernicus.org/articles/40/531/2022/>. 1

Burch, J. L., T. E. Moore, R. B. Torbert, and B. L. Giles, 2016. Magnetospheric Multiscale Overview and Science Objectives. *Space Science Reviews*, **199**(1-4), 5–21. 10.1007/s11214-015-0164-9. 1

Cao, J. B., Y. D. Ma, G. Parks, H. Reme, I. Dandouras, et al., 2006. Joint observations by Cluster satellites of bursty bulk flows in the magnetotail. *Journal of Geophysical Research: Space Physics*, **111**(A4). <https://doi.org/10.1029/2005JA011322>. 5

- Eggington, J. W. B., J. P. Eastwood, L. Mejnertsen, R. T. Desai, and J. P. Chittenden, 2020. Dipole Tilt Effect on Magnetopause Reconnection and the Steady-State Magnetosphere-Ionosphere System: Global MHD Simulations. *Journal of Geophysical Research: Space Physics*, **125**(7), e2019JA027,510. <https://doi.org/10.1029/2019JA027510>. 5
- Engebretson, M. J., S. A. Gaffaney, J. A. Ochoa, A. Runov, J. M. Weygand, et al., 2024. Signatures of Dipolarizing Flux Bundles in the Nightside Auroral Zone. *Journal of Geophysical Research: Space Physics*, **129**(4), e2023JA032,266. <https://doi.org/10.1029/2023JA032266>. 3.5
- Juusola, L., R. Nakamura, O. Amm, and K. Kauristie, 2009. Conjugate ionospheric equivalent currents during bursty bulk flows. *Journal of Geophysical Research: Space Physics*, **114**(A4). <https://doi.org/10.1029/2008JA013908>. 1
- Keiling, A., 2009. Alfvén waves and their roles in the dynamics of the Earth’s magnetotail: a review. *Space Science Reviews*, **142**, 73–156. 4
- Keiling, A., V. Angelopoulos, A. Runov, J. Weygand, S. V. Apatenkov, et al., 2009. Substorm current wedge driven by plasma flow vortices: THEMIS observations. *Journal of Geophysical Research: Space Physics*, **114**(A1). <https://doi.org/10.1029/2009JA014114>. 1
- Lanabere, V., L. Richard, and A. Dimmock, 2024. Database of MMS bursty bulk flows including their ionospheric foot-points. 10.5281/zenodo.13789048, URL <https://doi.org/10.5281/zenodo.13789048>. 2.3
- Liu, J., V. Angelopoulos, X. Chu, X.-Z. Zhou, and C. Yue, 2015. Substorm current wedge composition by wedgelets. *Geophysical Research Letters*, **42**(6), 1669–1676. 10.1002/2015GL063289. 1, B
- Liu, J., V. Angelopoulos, X.-Z. Zhou, A. Runov, and Z. Yao, 2013. On the role of pressure and flow perturbations around dipolarizing flux bundles. *Journal of Geophysical Research: Space Physics*, **118**(11), 7104–7118. <https://doi.org/10.1002/2013JA019256>. 3.5
- Nakamura, R., W. Baumjohann, R. Schödel, M. Brittnacher, V. A. Sergeev, M. Kubyshkina, T. Mukai, and K. Liou, 2001. Earthward flow bursts, auroral streamers, and small expansions. *Journal of Geophysical Research: Space Physics*, **106**(A6), 10,791–10,802. <https://doi.org/10.1029/2000JA000306>. 1
- Opgenoorth, H. J., M. A. Persson, T. I. Pulkkinen, and R. J. Pellinen, 1994. Recovery phase of magnetospheric substorms and its association with morning-sector aurora. *Journal of Geophysical Research*, **99**(A3). 10.1029/93JA01502. 1
- Panov, E. V., W. Baumjohann, R. Nakamura, P. L. Pritchett, J. M. Weygand, and M. V. Kubyshkina, 2019. Ionospheric Footprints of Detached Magnetotail Interchange Heads. *Geophysical Research Letters*, **46**(13), 7237–7247. <https://doi.org/10.1029/2019GL083070>. 1
- Peredo, M., D. P. Stern, and N. A. Tsyganenko, 1993. Are existing magnetospheric models excessively stretched? *Journal of Geophysical Research: Space Physics*, **98**(A9), 15,343–15,354. <https://doi.org/10.1029/93JA01150>. 5
- Pulkkinen, A., S. Lindahl, A. Viljanen, and R. Pirjola, 2005. Geomagnetic storm of 29–31 October 2003: Geomagnetically induced currents and their relation to problems in the Swedish high-voltage power transmission system. *Space Weather*, **3**(8), S08C03. 10.1029/2004SW000123. 1

- Qin, Z., R. E. Denton, N. A. Tsyganenko, and S. Wolf, 2007. Solar wind parameters for magnetospheric magnetic field modeling. *Space Weather*, **5**(11). <https://doi.org/10.1029/2006SW000296>. 2.2, 3.3
- Richard, L., Y. V. Khotyaintsev, D. B. Graham, and C. T. Russell, 2022a. Are Dipolarization Fronts a Typical Feature of Magnetotail Plasma Jets Fronts? *Geophysical Research Letters*, **49**(22), e2022GL101,693. <https://doi.org/10.1029/2022GL101693>. 2.1
- Richard, L., Y. V. Khotyaintsev, D. B. Graham, and C. T. Russell, 2022b. Are Dipolarization Fronts a Typical Feature of Magnetotail Plasma Jets Fronts? [Data set]. 10.5281/zenodo.7009706, URL <https://doi.org/10.5281/zenodo.7009706>. 2.1
- Rodger, C. J., D. H. Mac Manus, M. Dalzell, A. W. P. Thomson, E. Clarke, T. Petersen, M. A. Clilverd, and T. Divett, 2017. Long-Term Geomagnetically Induced Current Observations From New Zealand: Peak Current Estimates for Extreme Geomagnetic Storms. *Space Weather*, **15**(11), 1447–1460. 10.1002/2017SW001691. 1
- Runov, A., V. Angelopoulos, M. I. Sitnov, V. A. Sergeev, J. Bonnell, J. P. McFadden, D. Larson, K.-H. Glassmeier, and U. Auster, 2009. THEMIS observations of an earthward-propagating dipolarization front. *Geophysical Research Letters*, **36**(14). <https://doi.org/10.1029/2009GL038980>. 5
- Schillings, A., L. Palin, G. E. Bower, H. J. Opgenoorth, S. E. Milan, et al., 2023. Signatures of wedgelets over Fennoscandia during the St Patrick’s Day Storm 2015. *Journal of Space Weather and Space Climate*, **13**, 19. 10.1051/swsc/2023018. 1
- Tsyganenko, N., 1987. Global quantitative models of the geomagnetic field in the cislunar magnetosphere for different disturbance levels. *Planetary and Space Science*, **35**(11), 1347–1358. [https://doi.org/10.1016/0032-0633\(87\)90046-8](https://doi.org/10.1016/0032-0633(87)90046-8), URL <https://www.sciencedirect.com/science/article/pii/0032063387900468>. 1
- Tsyganenko, N. A., 1989. A magnetospheric magnetic field model with a warped tail current sheet. *Planetary and Space Science*, **37**(1), 5–20. 10.1016/0032-0633(89)90066-4. 1
- Tsyganenko, N. A., 1996. Effects of the solar wind conditions in the global magnetospheric configurations as deduced from data-based field models (Invited). In E. J. Rolfe and B. Kaldeich, eds., International Conference on Substorms, vol. 389 of *ESA Special Publication*, 181. 1
- Tsyganenko, N. A., 2002a. A model of the near magnetosphere with a dawn-dusk asymmetry 1. Mathematical structure. *Journal of Geophysical Research (Space Physics)*, **107**(A8), 1179. 10.1029/2001JA000219. 1
- Tsyganenko, N. A., 2002b. A model of the near magnetosphere with a dawn-dusk asymmetry 2. Parameterization and fitting to observations. *Journal of Geophysical Research (Space Physics)*, **107**(A8), 1176. 10.1029/2001JA000220. 1
- Tsyganenko, N. A., and M. I. Sitnov, 2005. Modeling the dynamics of the inner magnetosphere during strong geomagnetic storms. *Journal of Geophysical Research (Space Physics)*, **110**(A3), A03208. 10.1029/2004JA010798. 1
- Vasyliunas, V. M., J. R. Kan, G. L. Siscoe, and S. I. Akasofu, 1982. Scaling relations governing magnetospheric energy transfer. *Planetary and Space Science*, **30**(4), 359–365. 10.1016/0032-0633(82)90041-1. 3.3

- Wei, D., M. W. Dunlop, J. Yang, X. Dong, Y. Yu, and T. Wang, 2021. Intense dB/dt Variations Driven by Near-Earth Bursty Bulk Flows (BBFs): A Case Study. *Geophysical Research Letters*, **48**(4), e2020GL091781. <https://doi.org/10.1029/2020GL091781>. 1
- Weigel, R. S., D. Vassiliadis, and A. J. Klimas, 2002. Coupling of the solar wind to temporal fluctuations in ground magnetic fields. *Geophysical Research Letters*, **29**(19), 21–1–21–4. <https://doi.org/10.1029/2002GL014740>. 5
- Yamazaki, Y., J. Matzka, C. Stolle, G. Kervalishvili, J. Rauberg, O. Bronkalla, A. Morschhauser, S. Bruinsma, Y. Y. Shprits, and D. R. Jackson, 2022. Geomagnetic Activity Index Hpo. *Geophysical Research Letters*, **49**(10), e98860. [10.1029/2022GL098860](https://doi.org/10.1029/2022GL098860). 2.2